Chapter 6

Possible Evidence of CMEs Associated with Flares by Inferring Variations in Hydrogen Column Density

In this chapter, we investigate flare-associated coronal mass ejections (CMEs) in the active, fast-rotating star AB Doradus by examining temporal variations in the hydrogen column density (N_H) during X-ray flares. Using time-resolved spectral analysis, we detected significant enhancements in N_H coinciding with the peak phases of multiple, overlapping flares. In contrast, isolated single flares showed no such variation. These enhancements suggest the transient presence of cool, absorbing plasma along the line of sight during flare events, strongly indicating their physical association with the flares. We also verified the variation in N_H by applying the ice-cream cone model assuming a three-dimensional geometry. Based on the estimated flare loop dimensions and the ejected CME mass, the resulting N_H values ranged from 0.65 to 9.95×10^{20} cm^{-2}, aligning well with those obtained

through spectral modeling. This consistency provides strong observational support for the presence of failed eruptions or flare-associated CMEs.

6.1 Introduction

Coronal Mass Ejections (CMEs) are large-scale eruptions of magnetized plasma from a star's corona, often occurring alongside powerful flares and driven by the restructuring of magnetic fields through reconnection. On the Sun, CMEs are routinely observed using coronagraphs, with occurrence rates peaking at several events per day during solar maximum. These eruptions, especially during major flares, play a key role in solar and heliospheric dynamics. Extending this understanding to other stars, especially young and magnetically active solar analogues, has proven difficult due to the lack of direct imaging techniques. Despite this, several indirect methods such as Doppler-shifted Balmer line profiles, X-ray and UV blueshifted emission, and coronal dimming in EUV/X-ray have been employed to identify candidate stellar CMEs.

In particular, AB Doradus, a young, rapidly rotating K-type star with strong surface magnetic fields, has emerged as a promising candidate for studying stellar CMEs. Veronig et al. (2021) reported five significant coronal dimming events on AB Dor likely originating from polar active regions due to the star's inclination and rotation period. Such long-duration dimmings, especially in regions constantly in view, suggest failed or confined CMEs, influenced by AB Dor's intense global magnetic field. In a recent study, Strickert et al. (2024) investigated CMEs on AB Dor using MHD simulations with a flux rope model, motivated by coronal dimming evidence suggesting a high-latitude eruption continuously visible to the observer. Employing a Background Stellar Wind Model and a CME Eruption Model, the authors found that CMEs initiated in open magnetic field regions were more likely to erupt, whereas those in closed regions were often confined due to magnetic tension.

While these findings support the solar-stellar connection in eruptive activity, the challenge of directly observing stellar CMEs persists.

One promising approach for detecting stellar CMEs is through the analysis of temporal variations in hydrogen column density (N_H) during flares. N_H represents the number of hydrogen atoms per unit area along the line of sight and acts as a measure of absorbing material between the source and the observer. Moschou et al. (2017) demonstrated that a transient increase in N_H coinciding with a flare can be interpreted as evidence for additional intervening material, potentially from an eruptive CME crossing the line of sight. This method provides an indirect but effective diagnostic for detecting stellar CMEs in X-ray observations, especially in stars where direct imaging is not feasible.

In this chapter, we apply this technique to investigate flare-associated CMEs in the magnetically active star AB Doradus. Using time-resolved spectral analysis of XMM-Newton observations, we examine temporal variations in N_H during 13 flares across six observation sets.

6.2 Analysis and Results

For this study, we used the same dataset comprising six observation sets of AB Dor that include a total of 13 flares, as analyzed in Chapter 3. Our primary aim here is to investigate the variation in the hydrogen column density (N_H) across these flare events. To do this, we utilized the modeled PN spectra of each flare segment, as described in Section 3.3.2. Unlike the earlier analysis where N_H was fixed at a constant value, we re-fitted the spectra using the same three-temperature (3T) APEC model, but this time allowing N_H to vary freely while keeping all other parameters like temperatures, emission measures, and global abundances fixed to their previously obtained values. In this model, the first two thermal components served as proxies for the quiescent emission, while the third component accounted for the flare plasma. Additionally, we incorporated the cflux model to estimate the unabsorbed

flux, which was then used to compute the X-ray luminosity for each flare segment. The resulting variations in N_H for all observation sets are presented in Fig. 6.1.

6.3 Discussion and Conclusions

The variation of N_H can be taken as a proxy of coronal mass ejection (CME). Nonetheless, the fluctuation in absorption levels during the flare cannot be solely attributed to the Coronal Mass Ejection (CME) scenario. However, the gradual decrease in absorption as the flare subsides aligns with the occurrence of CMEs, thereby lending further support to this interpretation (Moschou et al., 2017). The average quiescent N_H was found to be 1.5×10^{20} cm^{-2} , whereas the N_H during the flare varied from $0.4 - 3.4 \times 10^{20}$ cm^{-2} . The extinction E(B-V) in the direction of AB Dor is estimated to be 0.07 (Schlafly and Finkbeiner, 2011). However, Gaia parallax of AB Dor suggests a distance of only 15 pc, so it is probable that the reddening of its light is insignificant or nonexistent, which is also evident from the maximum estimated value of E(B-V) for AB Dor as 0.0003 mag (Boro Saikia et al., 2018). The derived value of galactic N_H for AB Dor is also found to be one to two orders of magnitude lower than the N_H derived from X-ray spectral fitting. This suggests that the value of N_H obtained from X-ray spectra is solely due to local effects.

For the flares from sets S1 and S2, the N_H is found to be maximum near the flare peak. This could be probably due to the multiple flaring episodes, which either occurred simultaneously or one after the other. This is not evident in other isolated flares observed in other epochs. The N_H was also found to be increased during the post-flare phase of the flares F2, F4, and F5. Based on the solar CME data, the N_H was found to increase during the flare or post-flare phases and depends on the separation angle between CME and associated flare, location of CME, and line of sight (Aarnio et al., 2011; Yashiro et al., 2008). If we closely inspect the PN light curve of the post-flare phase of F2, we noticed a continuous dimming and sudden brightening. The enhancement of N_H and dimming of

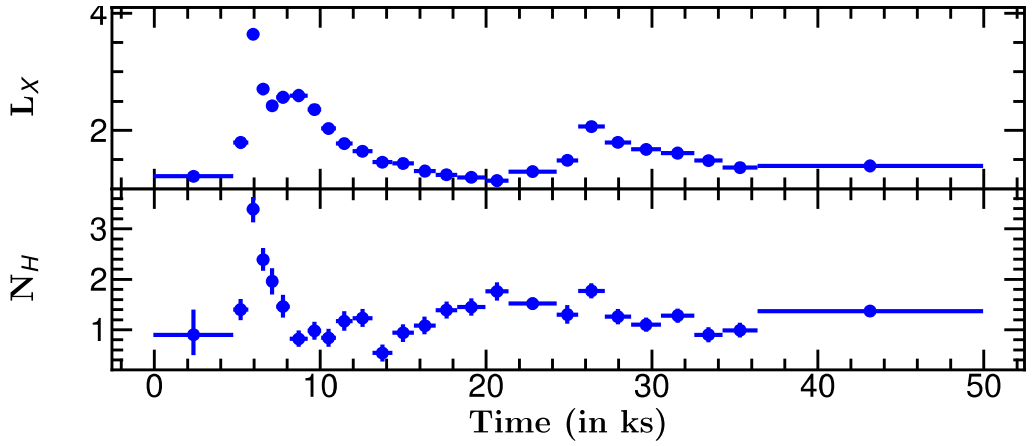

(a) set S1

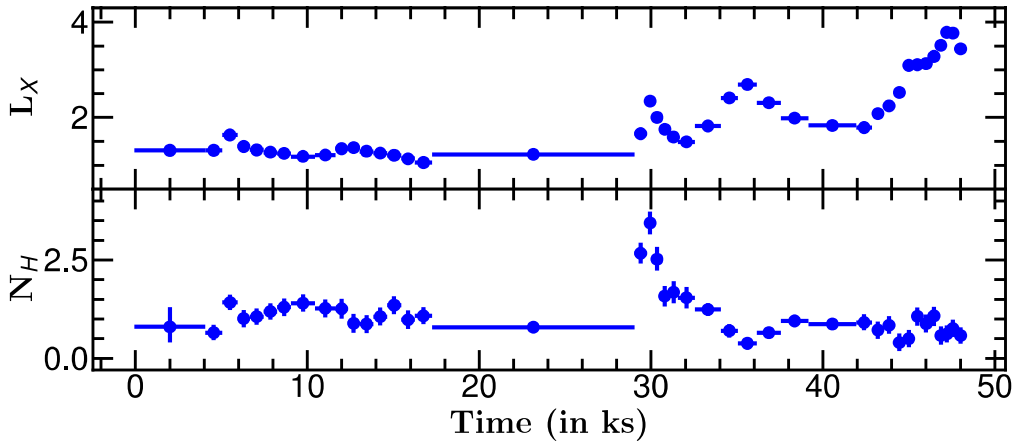

(b) set S2

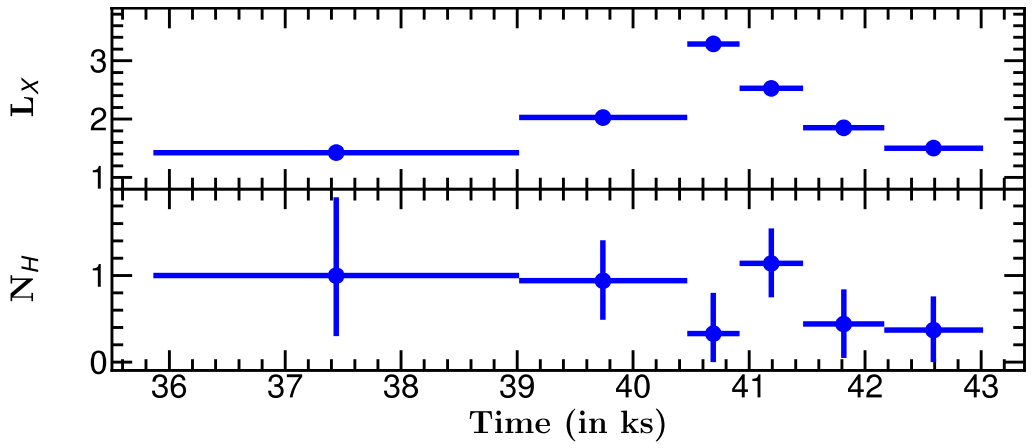

(c) set S3

Figure 6.1: Temporal evolution of the spectral parameters of AB Dor during flares and quiescent states showing X-ray luminosity in units of 10^{30} erg s^{-1} in top panel and hydrogen column density N_H in units of 10^{20} cm^{-2} in lower panel.

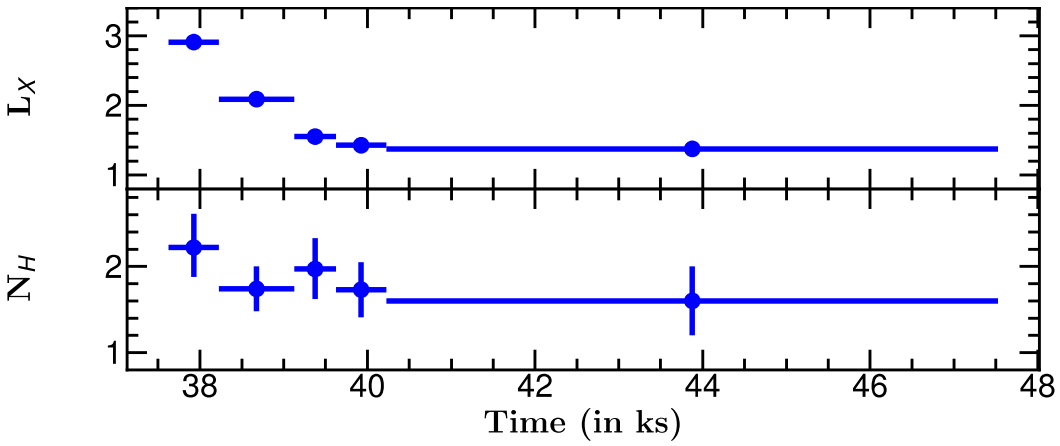

(d) set S4

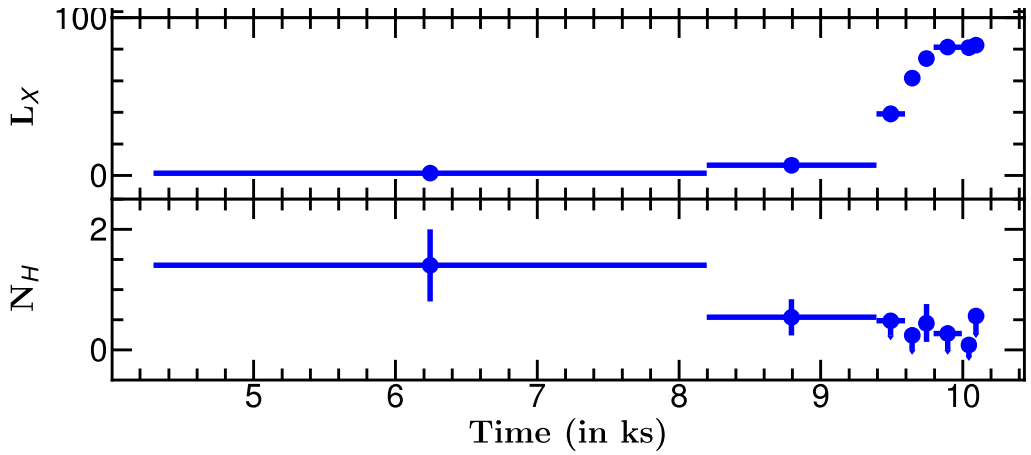

(e) set S5

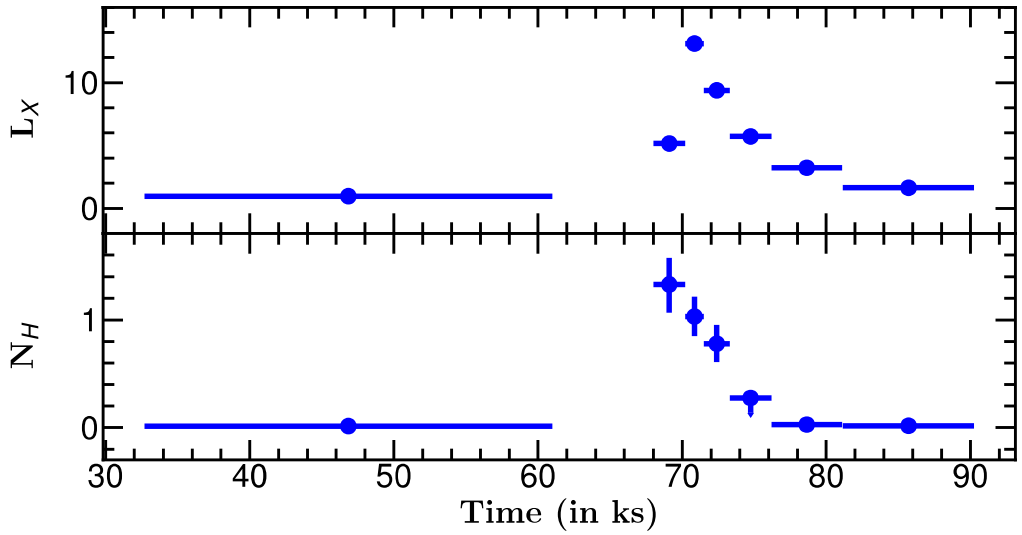

(f) set S6

Figure 6.1: Continued....

the light curve during the post-flare phases support the CME as suggested by (Veronig et al., 2021). After removing the effect of rotational modulation from set S2, we didn't see any strong signature of coronal dimming (See Fig. 3.2); however, the enhancement of N_H during the post-flare phases of flares F4 and F5 is indicative of CME. We suggest that the dimming in the light curve, along with the variation of N_H and removal of rotational modulation, will be useful criteria for detecting CME in solar-type stars.

An empirical relationship between the stellar flare energy in X-rays and its associated CME mass is estimated as $M_{CME}(g) = 10^{-1.5\pm0.5} E_G^{0.59\pm0.02}$, where E_G is the X-ray energy in GOES (1 – 8 Å) energy band (Aarnio et al., 2012; Drake et al., 2013). The derived X-ray flux is converted into GOES flux using WEBPIMMS for the derived flare temperatures of AB Dor. The estimated values of M_{CME} for AB Dor are found to be in the range 10^{18-19} g and are found to be maximum for the flare F15. These values of CMEs are 10 to 100 times more than the most massive solar CME (Yashiro and Gopalswamy, 2009) and similar to other stellar CMEs (Gunn et al., 1994; Karmakar et al., 2022; Namekata et al., 2021).

We have also estimated the absorption using the ice-cream cone model (Fisher and Munro, 1984) and equation 9 from Moschou et al. (2017). All the symbols used in this estimation are taken from Moschou et al. (2017).

The cone height can be estimated by using the equation $d(t) = (S(t) + R_{ABDor})/(tan(\omega + \phi) + 1)$, where S(t) represents the distance traveled by the plasma in time t. The lower and upper limits on S(t) are assumed as $0.2 \times R_*$ for flare and $15 \times R_*$ for dynamical length scale. From Table 3.4, we took the average half loop length as 2×10^{10} cm and the ejected mass (M_{obs}) as 3.24×10^{18} g. The estimated values of N_H ranged from 0.65 to 9.95×10^{20} cm^{-2} for the flare scenario and from 0.33 to 2.20×10^{20} cm^{-2} for the dynamical length scale scenario. These values were found to be consistent with the values obtained through the spectral fitting, as shown in Table 6.1.

Table 6.1: Best fit spectral parameters of each temporal segment of the flares F1-F10, F13, F15, and F20. Here, FS represents flare segments, and ST and ET refer to the start and end times, respectively of each flare segment relative to the start time of the corresponding observation.

Set	Flare	FS	ST:ET (ks)	N_H (10^{20} cm^{-2})	L_{XF} (10^{30} erg s^{-1})	χ^2_ν (dof)
S1	F1	R	4.8 : 5.7	$1.4^{+0.2}_{-0.2}$	$1.79^{+0.01}_{-0.01}$	1.08 (351)
		P	5.7 : 6.3	$3.4^{+0.2}_{-0.3}$	$3.64^{+0.02}_{-0.02}$	1.19 (425)
		D1	6.3 : 6.9	$2.4^{+0.2}_{-0.2}$	$2.71^{+0.02}_{-0.02}$	1.19 (349)
		D2	6.9 : 7.4	$2.0^{+0.3}_{-0.3}$	$2.42^{+0.02}_{-0.02}$	0.95 (316)
	F2	R	7.4 : 8.2	$1.5^{+0.2}_{-0.2}$	$2.57^{+0.02}_{-0.02}$	1.02 (359)
		P	8.2 : 9.3	$0.8^{+0.2}_{-0.2}$	$2.60^{+0.01}_{-0.01}$	1.00 (431)
		D1	9.3 : 10.1	$1.0^{+0.2}_{-0.2}$	$2.36^{+0.01}_{-0.01}$	0.96 (373)
		D2	10.1 : 11.0	$0.8^{+0.2}_{-0.2}$	$2.04^{+0.01}_{-0.01}$	1.16 (364)
		D3	11.0 : 12.0	$1.2^{+0.2}_{-0.2}$	$1.78^{+0.01}_{-0.01}$	1.28 (349)
		D4	12.0 : 13.2	$1.2^{+0.2}_{-0.2}$	$1.65^{+0.01}_{-0.01}$	1.04 (358)
		D5	13.2 : 14.4	$0.5^{+0.2}_{-0.2}$	$1.457^{+0.009}_{-0.009}$	1.04 (342)
		D6	14.4 : 15.7	$0.9^{+0.2}_{-0.2}$	$1.436^{+0.009}_{-0.009}$	1.10 (348)
		D7	15.7 : 17.0	$1.1^{+0.2}_{-0.2}$	$1.305^{+0.008}_{-0.009}$	1.03 (329)
		D8	17.0 : 18.3	$1.4^{+0.2}_{-0.2}$	$1.241^{+0.008}_{-0.008}$	1.01 (335)
		D9	18.3 : 20.0	$1.4^{+0.2}_{-0.2}$	$1.197^{+0.007}_{-0.008}$	1.04 (327)
		D10	20.0 : 21.4	$1.8^{+0.2}_{-0.2}$	$1.141^{+0.008}_{-0.008}$	1.11 (309)
	F3	R	24.3 : 25.6	$1.3^{+0.2}_{-0.2}$	$1.489^{+0.009}_{-0.009}$	1.11 (357)
		P	25.6 : 27.2	$1.8^{+0.1}_{-0.1}$	$2.07^{+0.01}_{-0.01}$	1.27 (445)
		D1	27.2 : 28.8	$1.3^{+0.1}_{-0.1}$	$1.796^{+0.009}_{-0.009}$	1.24 (413)
		D2	28.8 : 30.6	$1.1^{+0.1}_{-0.1}$	$1.677^{+0.008}_{-0.008}$	1.13 (417)

Continued on next page

Table 6.1 – continued from previous page

Set	Flare	FS	ST:ET (ks)	N_H (10^{20} cm^{-2})	L_{XF} (10^{30} erg s^{-1})	χ^2_ν (dof)
		D3	30.6 : 32.6	$1.3^{+0.1}_{-0.1}$	$1.612^{+0.008}_{-0.008}$	1.16 (427)
		D4	32.6 : 34.3	$0.9^{+0.2}_{-0.2}$	$1.484^{+0.008}_{-0.008}$	1.04 (385)
		D5	34.3 : 36.4	$1.0^{+0.1}_{-0.1}$	$1.364^{+0.007}_{-0.007}$	1.04 (390)
S2	F4	R	4.1 : 5.1	$0.6^{+0.2}_{-0.2}$	$1.311^{+0.009}_{-0.01}$	1.17 (298)
		P	5.1 : 6.0	$1.4^{+0.2}_{-0.2}$	$1.63^{+0.01}_{-0.01}$	1.15 (333)
		D1	6.0 : 6.7	$1.0^{+0.2}_{-0.2}$	$1.39^{+0.01}_{-0.01}$	1.09 (280)
		D2	6.7 : 7.5	$1.1^{+0.2}_{-0.2}$	$1.32^{+0.01}_{-0.01}$	1.01 (286)
		D3	7.5 : 8.3	$1.2^{+0.2}_{-0.2}$	$1.27^{+0.01}_{-0.01}$	1.09 (280)
		D4	8.3 : 9.1	$1.3^{+0.2}_{-0.2}$	$1.24^{+0.01}_{-0.01}$	1.28 (278)
		D5	9.1 : 10.5	$1.4^{+0.2}_{-0.2}$	$1.182^{+0.009}_{-0.009}$	1.14 (275)
	F5	R1	10.5 : 11.7	$1.3^{+0.2}_{-0.2}$	$1.21^{+0.01}_{-0.01}$	0.99 (261)
		R2	11.7 : 12.4	$1.3^{+0.2}_{-0.2}$	$1.35^{+0.01}_{-0.01}$	1.07 (264)
		P	12.4 : 13.1	$0.9^{+0.2}_{-0.2}$	$1.37^{+0.01}_{-0.01}$	1.05 (263)
		D1	13.1 : 13.9	$0.9^{+0.2}_{-0.2}$	$1.29^{+0.01}_{-0.01}$	1.05 (274)
		D2	13.9 : 14.7	$1.1^{+0.2}_{-0.2}$	$1.25^{+0.01}_{-0.01}$	1.08 (266)
		D3	14.7 : 15.5	$1.3^{+0.2}_{-0.2}$	$1.21^{+0.01}_{-0.01}$	1.03 (258)
		D4	15.5 : 16.3	$1.0^{+0.2}_{-0.2}$	$1.14^{+0.01}_{-0.01}$	1.18 (250)
		D5	16.3 : 17.3	$1.1^{+0.2}_{-0.2}$	$1.055^{+0.008}_{-0.008}$	1.17 (258)
	F6	R	29.1 : 29.8	$2.7^{+0.3}_{-0.3}$	$1.66^{+0.01}_{-0.01}$	1.29 (301)
		P	29.8 : 30.2	$3.4^{+0.3}_{-0.3}$	$2.34^{+0.02}_{-0.02}$	1.13 (310)
		D1	30.2 : 30.6	$2.5^{+0.3}_{-0.3}$	$2.00^{+0.02}_{-0.02}$	1.17 (287)
		D2	30.6 : 31.1	$1.6^{+0.3}_{-0.3}$	$1.75^{+0.01}_{-0.01}$	1.00 (289)

Continued on next page

Table 6.1 – continued from previous page

Set	Flare	FS	ST:ET (ks)	N_H (10^{20} cm^{-2})	L_{XF} (10^{30} erg s^{-1})	χ^2_ν (dof)
		D3	31.1 : 31.6	$1.7^{+0.3}_{-0.3}$	$1.59^{+0.01}_{-0.01}$	1.01 (277)
		D4	31.6 : 32.6	$1.5^{+0.3}_{-0.3}$	$1.49^{+0.01}_{-0.01}$	1.05 (268)
	F7	R1	32.6 : 34.1	$1.2^{+0.2}_{-0.2}$	$1.8^{+0.01}_{-0.01}$	1.14 (434)
		R2	34.1 : 35.1	$0.7^{+0.2}_{-0.2}$	$2.41^{+0.01}_{-0.01}$	1.05 (453)
		P	35.1 : 36.2	$0.4^{+0.2}_{-0.1}$	$2.70^{+0.01}_{-0.01}$	1.19 (488)
		D1	36.2 : 37.6	$0.6^{+0.1}_{-0.1}$	$2.31^{+0.01}_{-0.01}$	1.27 (482)
		D2	37.6 : 39.2	$0.9^{+0.1}_{-0.1}$	$1.984^{+0.009}_{-0.009}$	1.04 (460)
		D3	39.2 : 42.0	$0.9^{+0.1}_{-0.1}$	$1.831^{+0.009}_{-0.009}$	1.12 (457)
	F8	R1	42.0 : 42.9	$0.9^{+0.2}_{-0.2}$	$1.79^{+0.01}_{-0.01}$	1.03 (327)
		R2	42.9 : 43.6	$0.7^{+0.2}_{-0.2}$	$2.08^{+0.01}_{-0.01}$	1.11 (342)
		R3	43.6 : 44.2	$0.8^{+0.2}_{-0.2}$	$2.24^{+0.02}_{-0.02}$	1.09 (332)
		R4	44.2 : 44.8	$0.4^{+0.2}_{-0.2}$	$2.52^{+0.02}_{-0.02}$	1.09 (360)
		R5	44.8 : 45.3	$0.5^{+0.2}_{-0.2}$	$3.09^{+0.02}_{-0.02}$	1.10 (376)
		P	45.3 : 45.8	$1.1^{+0.2}_{-0.2}$	$3.11^{+0.02}_{-0.02}$	1.19 (369)
		D	45.8 : 46.3	$0.9^{+0.2}_{-0.2}$	$3.13^{+0.02}_{-0.02}$	0.97 (368)
	F9	R1	46.3 : 46.7	$1.1^{+0.2}_{-0.3}$	$3.28^{+0.02}_{-0.03}$	1.03 (339)
		R2	46.7 : 47.1	$0.6^{+0.2}_{-0.2}$	$3.52^{+0.03}_{-0.03}$	1.06 (356)
		R3	47.1 : 47.4	$0.6^{+0.2}_{-0.2}$	$3.79^{+0.03}_{-0.03}$	1.27 (371)
		P	47.4 : 47.8	$0.8^{+0.2}_{-0.2}$	$3.77^{+0.03}_{-0.03}$	0.92 (366)
		D	47.8 : 48.2	$0.6^{+0.2}_{-0.2}$	$3.44^{+0.03}_{-0.02}$	1.02 (355)
S3	F10	R	39.04 : 40.49	$0.9^{+0.5}_{-0.4}$	$2.03^{+0.03}_{-0.03}$	0.89 (208)
		P	40.49 : 40.94	$0.3^{+0.5}_{-0.3}$	$3.29^{+0.04}_{-0.04}$	1.04 (230)

Continued on next page

Table 6.1 – continued from previous page

Set	Flare	FS	ST:ET (ks)	N_H (10^{20} cm^{-2})	L_{XF} (10^{30} erg s^{-1})	χ^2_ν (dof)
		D1	40.94 : 41.49	$1.1^{+0.4}_{-0.4}$	$2.53^{+0.03}_{-0.03}$	1.16 (252)
		D2	41.49 : 42.19	$0.4^{+0.4}_{-0.3}$	$1.85^{+0.02}_{-0.02}$	1.09 (228)
		D3	42.19 : 43.04	$0.4^{+0.4}_{-0.3}$	$1.50^{+0.02}_{-0.02}$	0.94 (216)
S4	F13	D1	37.63 : 38.23	$2.2^{+0.3}_{-0.3}$	$2.91^{+0.02}_{-0.02}$	0.88 (268)
		D2	38.23 : 39.19	$1.7^{+0.3}_{-0.3}$	$2.09^{+0.01}_{-0.01}$	1.03 (270)
		D3	39.19 : 39.63	$2.0^{+0.4}_{-0.4}$	$1.55^{+0.02}_{-0.02}$	1.16 (239)
		D4	39.63 :40.23	$1.7^{+0.3}_{-0.3}$	$1.43^{+0.01}_{-0.01}$	1.08 (243)
S5	F15	R1	8.19 : 9.39	$0.5^{+0.3}_{-0.3}$	$6.48^{+0.05}_{-0.05}$	1.03 (411)
		R2	9.39 : 9.59	<0.5	$39.0^{+0.3}_{-0.3}$	1.09 (561)
		R3	9.59 : 9.69	<0.2	$61.7^{+0.4}_{-0.4}$	1.14 (557)
		R4	9.69 : 9.79	$0.4^{+0.3}_{-0.3}$	$74.1^{+0.6}_{-0.6}$	1.20 (472)
		R5	9.79 : 9.99	<0.3	$81.3^{+0.6}_{-0.6}$	1.05 (532)
		R6	9.99 : 10.09	<0.1	$81.1^{+0.7}_{-0.7}$	1.11 (432)
		P	10.09 : 10.19	<0.6	$82.6^{+0.7}_{-0.7}$	1.14 (451)
	*F15	R	8.70 : 10.10	$2.9^{+0.2}_{-0.2}$	$20.3^{+0.1}_{-0.1}$	1.10 (1342)
		P	10.10 : 10.90	$2.1^{+0.1}_{-0.1}$	$46.5^{+0.2}_{-0.2}$	1.27 (1778)
		D1	10.90 : 12.00	$2.2^{+0.1}_{-0.1}$	$33.6^{+0.2}_{-0.2}$	1.63 (1610)
		D2	12.00 : 14.00	$1.8^{+0.1}_{-0.1}$	$16.24^{+0.08}_{-0.08}$	1.79 (1744)
S6	*F20	R	68.0 : 70.2	$1.3^{+0.2}_{-0.3}$	$5.16^{+0.04}_{-0.04}$	1.10 (656)
		P	70.2 : 71.5	$1.0^{+0.2}_{-0.2}$	$13.11^{+0.09}_{-0.09}$	1.26 (905)
		D1	71.5 : 73.3	$0.8^{+0.2}_{-0.2}$	$9.38^{+0.06}_{-0.06}$	1.63 (924)
		D2	73.3 : 76.2	< 0.28	$5.72^{+0.04}_{-0.04}$	1.71 (962)

Continued on next page

Table 6.1 – continued from previous page

Set	Flare	FS	ST:ET (ks)	N_H (10^{20} cm^{-2})	L_{XF} (10^{30} erg s^{-1})	χ^2_ν (dof)
		D3	76.2 : 81.1	< 0.03	$3.23^{+0.02}_{-0.02}$	1.60 (947)
		D4	81.1 : 90.3	< 0.02	$1.64^{+0.01}_{-0.01}$	1.32 (948)